

Tracking Outflow using Line-Locking (TOLL). II. Large Line-Locking Web identified in Quasar J151352+085555

CHEN CHEN,¹ ZHICHENG HE,² WEIMIN YI,³ TUO JI,⁴ MARIE WINGYEE LAU,⁵ AND BO MA^{6,7}

¹*Zhuhai College of Science and Technology, Zhuhai 519000, China*

²*CAS Key Laboratory for Research in Galaxies and Cosmology, Department of Astronomy, University of Science and Technology of China, Hefei 230026, China*

³*Yunnan Observatories, Kunming 650216, China*

⁴*Center for Space Physics and Astronomy, Key Laboratory for Polar Science of the State Oceanic Administration, Polar Research Institute of China, Shanghai 200136, People's Republic of China*

⁵*Department of Physics and Astronomy, University of California Riverside, Riverside, CA 92507, USA*

⁶*School of Physics & Astronomy, Sun Yat-Sen University, Zhuhai 519000, China*

⁷*CSST Science Center in the Great Bay Area, Sun Yat-sen University, Zhuhai 519000, China*

(Received; Revised; Accepted)

Submitted to ApJ

ABSTRACT

Quasar outflows often consist of two clouds with velocity separations matching the doublet spacings of common UV resonance transitions, a phenomenon known as line-locking, which is commonly observed in quasar spectra. Multiple clouds can be locked together through multi-ion doublets, forming ‘line-locking web’. In the second paper of the TOLL project, we present discovery of one of the largest ‘line-locking web’ known to date from the VLT/UVES spectra of QSO J151352+085555. We identify 12 associated narrow absorption line systems through the C IV, N V, Si IV, O VI, and multiple Lyman lines (Ly α to Ly ϵ), and find 10 out of the 12 absorbers are line-locked together by comparing velocity separations between different absorption systems. By conducting photoionization modeling with CLOUDY, we measure the total hydrogen column densities, metallicities, and ionization parameters of these absorbers, which suggests the absorbers likely have sub-solar metallicities. A preliminary statistical analysis demonstrates the shadowed clouds tend to have similar ionization states comparing to the shadowing ones. Identification of one of the largest line-locking webs implies that radiative acceleration plays an important role in sorting out cloud velocities in quasar outflows, and highlights the need for more sophisticated theoretical models to explain its formation and evolution.

1. INTRODUCTION

Quasar outflows play a crucial role in galaxy evolution by providing kinetic energy feedback from central supermassive black holes to their host galaxies (Silk & Rees 1998; Kauffmann & Haehnelt 2000; Berti & Volonteri 2008; Costa et al. 2014; Barai et al. 2016; Anglés-Alcázar et al. 2017a,b; Barai & de Gouveia Dal Pino 2019; Bustamante & Springel 2019; He et al. 2022; Chen et al. 2022; Bluck et al. 2023; Ayubinia et al. 2023; Naddaf et al. 2023; Hall et al. 2024; He et al. 2024; Bollati et al. 2024). Several possible outflow/wind driving mechanisms, including thermal process, radiation pres-

sure, and magnetic fields, have been investigated extensively (Mushotzky et al. 1972; Scargle 1973; Begelman et al. 1983; Krolik & Begelman 1986; Camenzind 1986; Pelletier & Pudritz 1992; Netzer & Laor 1993; Arav et al. 1994, 1995; de Kool & Begelman 1995; Murray et al. 1995; Proga et al. 2000; Proga & Kallman 2004; Chelouche & Netzer 2005; Netzer 2006; Proga 2007; Baskin & Laor 2012; Baskin et al. 2014; Netzer et al. 2024). One common and distinctive feature observed in these outflows, which is often considered as evidence supporting the radiation pressure mechanism, is line-locking (Milne 1926; Scargle 1973; Burbidge & Burbidge 1975; Goldreich & Sargent 1976; Foltz et al. 1987; Braun & Milgrom 1989). It is a phenomenon where the velocity difference between two different absorption components matches the separation of known atomic doublet transi-

tions, like the C IV doublets (Foltz et al. 1987; Srianand et al. 2002; Ganguly et al. 2003; Gallagher et al. 2004; Hamann et al. 2011; Bowler et al. 2014; Chen et al. 2019; Lin & Lu 2020a,b; Lu & Lin 2020; Chen et al. 2024). In the geometrical configuration, the slower (shadowing) component lies between the emission source and the other faster (shadowed) outflow component. This configuration will be maintained as long as the acceleration of the shadowed component via radiation pressure through the red doublet stays equal to or greater than what the acceleration difference between the two outflow components would be outside of the shadow. Thus, studying line-locking can provide valuable insights into the role of radiation pressure played in driving and shaping quasar outflows.

The formation and evolution of line-locking between two absorbing clouds through two resonance lines in active galaxies has been explored theoretically. For instance, Braun & Milgrom (1989) proposed a popular non-steady state mechanism to explain the formation of line-locking. Korista et al. (1993) provided a detailed analysis of the line lock theory in BALQSOs, suggesting that radiation pressure and line-locking may play crucial roles in the formation of the observed double troughs in the C IV 1549 region, and has significant implications for understanding the dynamics of BAL outflows. Arav & Begelman (1994) provided a dynamical model that links the observed double troughs in the C IV BAL of BALQSOs to the modulation of the radiative force due to line locking between Ly α and N V λ 1240 resonance lines (see also Arav 1996). Proga et al. (2000) extended previous models of line-driven winds, originally developed for hot stars, to the axially symmetric geometry of accretion disks in AGN. Vilkoviskij & Irwin (2001) showed that theories based on small cloud velocity interactions via line locking can explain the spectral observation of the BALQSO Q1303+1308. Chelouche & Netzer (2003) modeled the impact of shielding on properties of outflows, and found moderate shielding is especially efficient in accelerating flows to high velocities because of the suppression of gas ionization level. Baskin & Laor (2012) utilized a ‘metal ion runaway’ model to explain the apparent lack of Ly α -N V line-locking signature in C IV absorption troughs of some AGNs. Lewis & Chelouche (2023) studied a simplified two-clouds-one-doublet model and found that fine-tuning of physical parameters such as column density and ionization is required for line-locking to occur.

However, in practice, multiple clouds have been observed to be locked together through multi-ion doublets rather than just two clouds, and whether fine-tuning is needed in such cases remains questionable (Chen et al.

2024). For example, Hamann et al. (2011) detected 3 narrow absorption line systems (NALs) toward a quasar, line-locked together by the C IV doublet (see also Lin & Lu 2020a,b; Lu & Lin 2020; Chen et al. 2021a; Yi et al. 2024; Chen et al. 2024). For simplicity, we hereafter use the new concept of ‘line-locking web’ to describe the structure of the interconnected line-locking clouds in a quasar outflow. To study the formation and evolution of the line-locking web and develop more realistic theoretical models, we have initiated the Tracking Outflow using Line-Locking (TOLL) project (Chen et al. 2024, hereafter Paper I). The primary goal of the TOLL project is to first establish a well-characterized sample of line-locked systems using high resolution quasar spectra, and then conduct statistical and theoretical work based on the sample in the future. In the second paper of the TOLL project, we present identification of one of the largest line-locking web using high-resolution spectra of quasar J151352+085555 and conduct a statistical test of the ‘fine-tuning’ scenario proposed by Lewis & Chelouche (2023) using data from this and our previous works (Chen et al. 2018, 2019, 2024).

The outflow of quasar J151352+085555 was investigated by Srianand et al. (2002), where they have identified line-locking signatures corresponding to the O VI, N V, and C IV doublet splittings. In this paper, we re-analyze the UVES spectra of quasar J151352+085555 and report new findings in terms of its line-locking signatures. The structure of the paper is organized as follows. Section 2 introduces the UVES spectrum of J151352+085555 and the methodology for fitting line profiles of associated absorption lines (AALs; Weymann et al. 1979; Foltz et al. 1986; Anderson et al. 1987; Weymann et al. 1991; Hamann 1997), used to measure the Doppler parameters, column densities, velocity shifts, and covering fractions of each absorber. In Section 3, we describe results from line fitting, line-lock searching, and photoionization modeling. Section 4 compares our findings with results of Srianand et al. (2002), and discusses the implications of our results. Finally, Section 5 provides a summary of this work.

Throughout this paper, we adopt a cosmological model with $H_0 = 71 \text{ km s}^{-1} \text{ Mpc}^{-1}$, $\Omega_M = 0.27$, and $\Omega_\Lambda = 0.73$.

2. QUASAR SPECTRA AND DATA ANALYSIS

2.1. Quasar Spectra

The TOLL project’s parent sample of quasars is based on the catalog compiled by Chen et al. (2021b), which includes observations from VLT-UVES (Murphy et al. 2019) and Keck-HIRES (O’Meara et al. 2015). These spectra have resolutions ranging from $22,000 \lesssim R \lesssim$

71,000 for VLT-UVES. In the [Chen et al. \(2021b\)](#) study, each candidate mini-broad absorption line (mini-BAL) system was carefully examined to ensure it was not contaminated by unrelated intervening absorption features, such as damped Ly α or Lyman limit systems originating from foreground galaxies or their extended halos (e.g., [Prochaska et al. 2015](#); [Berg et al. 2015](#); [Prochaska et al. 2008](#)). Our main goal is to study these line-locked features in order to gain deeper insights into the dynamics of quasar outflows. Thus, we conducted a thorough visual inspection of both the normalized and unnormalized spectra of all quasars in the catalog, and selected J151352+085555 for its promising potential to reveal line-locked systems.

Quasar J151352+085555 (also named Q1511+091, SDSS J151352.52+085555.7) is optically bright ($m_B = 18.0$) and has a emission redshift of $z = 2.901$ measured from SDSS ([Abolfathi et al. 2018](#); [Pâris et al. 2018](#)). It is classified as a C IV broad absorption line (BAL) quasar, and has a bolometric luminosity of $10^{14} L_\odot$ and virial black hole mass of $2.5 \times 10^{10} M_\odot$ ([Shen et al. 2011](#); [Weedman et al. 2012](#)). [Sargent et al. \(1988\)](#) studied its C IV absorption using the Palomar 5m Hale Telescope, and found a strong complex absorption line system at a absorption redshift of $z_{obs} \sim 2.85$. It was found to be radio intermediate from the VLA FIRST survey, having a radio loudness of 1.34, and was given the name of FIRST J151352.5+085554 ([Helfand et al. 2015](#); [Shaban et al. 2022a](#)). A point source, CXOG J151352.5+085555, was detected in the X-ray band by Chandra near the optical position of quasar J151352+085555, with an variability amplitude about 50% and an average X-ray luminosity of $4 \times 10^{45} \text{ erg s}^{-1}$ (0.5-7 keV, [Wang et al. 2016](#); [Shaban et al. 2022b](#); [Quintin et al. 2024](#)).

UVES is a dual-arm, grating cross-dispersed high-resolution optical echelle spectrograph mounted on the Nasmyth B focus of Unit Telescope 2 of the VLT ([Dekker et al. 2000](#)). The UVES observations of quasar J151352+085555 (PI: Srianand; ProgramID: 65.P-0038, 69.B-0108, 71.B-0136) were conducted in 2000, 2002 and 2003 under a medium seeing of 0.56 arcsec, with a total on-target exposure time of 52713 seconds (see also [Murphy et al. 2019](#)). Seventeen exposures were taken in the UVES standard configuration using the 0.8" and 1" slit, providing a spectral resolution of $R \sim 50,000$ and wavelength coverage of 3284–10429 Å. [Murphy et al. \(2019\)](#) reduced the data using a modified version of the UVES reduction pipeline based on the optimally extracted method ([Horne 1986](#); [Piskunov & Valenti 2002](#); [Zechmeister et al. 2014](#); [Ma & Ge 2019](#)). The wavelength calibration is done using a single ThAr exposure ([Murphy et al. 2007](#)). We show the target

spectrum at the rest-frame wavelengths in Figure 1. We did not detect significant time-variable absorption lines from the spectra taken about three years apart. Different observations then were combined to form a single spectrum with a dispersion of 2.5 km s^{-1} per pixel. The final continuum-normalized spectrum has a count-to-noise ratio of 19, 40, 77, 78, and 52 per pixel (2.5 km s^{-1}) near 3500, 4500, 5500, 6500, and 7500 Å in the observed frame.

2.2. Line Profile Fitting

We use a standard fitting procedure to extract all relevant absorption line systems from the quasar spectra ([Chen et al. 2018, 2019, 2021b](#)). The fitting process begins with a thorough examination of the continuum placement provided in the UVES archive spectra for each line of interest. In cases where the continuum appears to be poorly constrained or exhibits sharp variations compared to the unnormalized spectrum, we refit the continuum using a locally-constrained simple power law. Then we start to identify individual velocity components in the associated absorption line (AAL) complexes, beginning with the C IV $\lambda 1548, 1551$ doublet. This doublet is typically strong in our target spectra, occupies wavelength range outside of the Lyman forest, and has a high signal-to-noise ratio. We then search for a wide range of other plausible lines at the corresponding redshifts to the C IV doublets, such as Si IV $\lambda 1394, 1403$, N V $\lambda 1239, 1243$, O VI $\lambda 1032, 1038$, and the Lyman series. Upon identifying new components at the redshifts associated with other absorption lines, we proceeded to verify the presence of corresponding C IV lines in return. This process of mutual validation continued until we had thoroughly cataloged all the lines involved. Our spectra include the AAL complexes of C IV, Si IV, O VI, and N V doublets. In some cases, other lines help confirm the positions of C IV components. For instance, component 5 in Figure 2 are identified through Si IV. Table 1 lists all identified lines in the quasar spectra.

Our line-fitting procedure follows the approach detailed in [Chen et al. \(2018, 2019\)](#). We fit each candidate AAL for C IV, Si IV, O VI, N V and the Lyman series using a Gaussian optical depth profile:

$$\tau_v = \tau_0 \exp\left(-\frac{(v - v_0)^2}{b^2}\right), \quad (1)$$

where τ_v is the optical depth at velocity v , τ_0 is the central optical depth, v_0 is the line center velocity, and b is the Doppler parameter. The two lines in each doublet are fit simultaneously, sharing the same velocity shift and b value. This procedure can also apply to the multiple lines in Lyman series, as they also share the same velocity shift and b value.

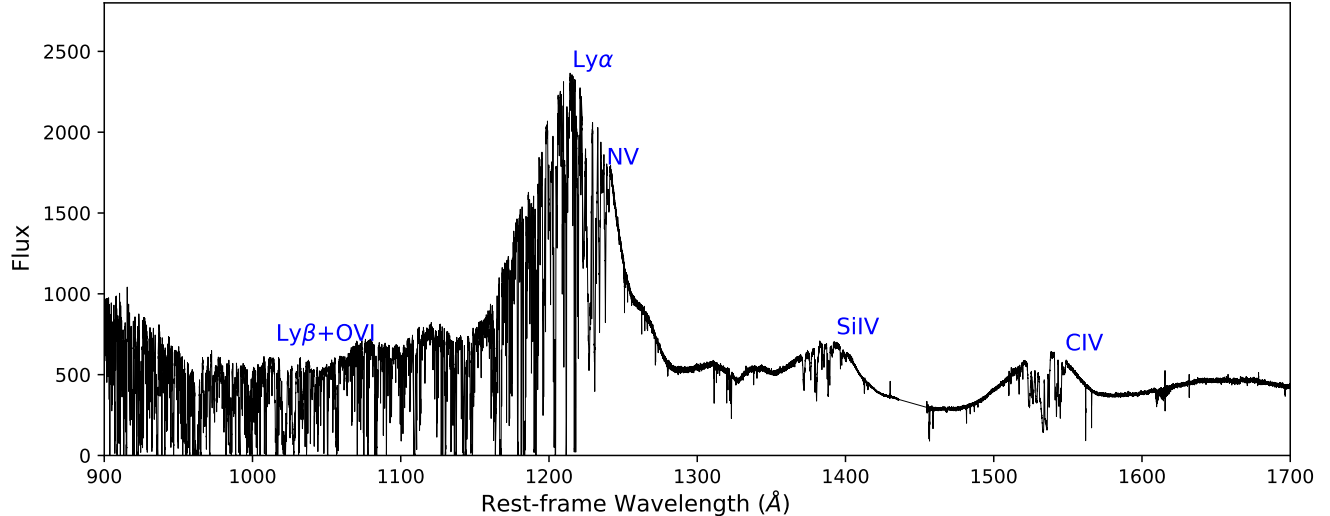


Figure 1. UVES spectrum of J151352+085555 at the rest-frame wavelengths (defined by the emission redshift $z = 2.901$) showing the absorption lines relative to the broad emission lines. The main emission lines are labeled across the top.

We account for partial coverage of the background light source in the fitting, assuming a spatially uniform brightness of the source and a homogeneous absorbing medium. The observed intensity at velocity v is then expressed as:

$$\frac{I_v}{I_0} = 1 - C_0 + C_0 \exp(-\tau_v), \quad (2)$$

where I_0 is the continuum intensity, I_v is the measured intensity at velocity v , and C_0 is the covering fraction along our line of sight, with $0 < C_0 \leq 1$ (Ganguly et al. 1999; Hamann et al. 1997; Barlow et al. 1997). We assume a constant covering fraction across the AAL profiles, attributed to the narrowness of the lines and the minimal variation in their lower extremities. But the value of C_0 can differ between lines.

The column densities for C IV, Si IV, O VI, and NV are derived from the fitted optical depths using the relation:

$$\tau_0 = \frac{\sqrt{\pi} e^2}{m_e c} \frac{N_i f_{\text{oscillator}} \lambda_0}{b}, \quad (3)$$

where N_i is the ion column density, $f_{\text{oscillator}}$ is the oscillator strength, λ_0 is the rest wavelength, and b is the Doppler parameter.

While most fits are straightforward, certain lines present challenges due to blending with other absorption systems or unrelated lines. When multiple systems are blended, we fit the doublets simultaneously and resolve individual AALs only if they can be clearly distinguished visually. For regions containing unrelated absorption at different redshifts, we mask these areas before conduct the fitting procedure. Most O VI lines are heavily contaminated within the Ly α to Ly ϵ forests. We estimate

their lower limits for conservation. For the components that show multiple Lyman lines, we try to fit as many Lyman lines as possible simultaneously to get the best constraints on the column densities and covering fractions.

3. RESULTS

3.1. Line Fitting Parameters

The fitted line parameters and corresponding uncertainties of the C IV, Si IV, O VI, and NV doublets from the VLT-UVES spectrum of quasar J151352+085555 are summarized in Table 1. The table presents the measured quantities for each line, including the velocity shift v , line identification, rest wavelength, observed wavelength, Doppler parameter b , logarithm of the column density, and covering fraction C_0 . These measurements are provided separately for the C IV, Si IV, O VI, and NV doublets. The last column contains notes regarding any line blends. The data are organized by redshift, corresponding to the component numbers listed in the first column, as shown in Figures 2 to 6. The uncertainties reported for most parameters represent the 1σ errors obtained from the fitting procedure, primarily reflecting pixel-to-pixel noise in the spectra. For cases of significant blending, we employ the methods outlined in Section 3.2 of Chen et al. (2018) and Section 3.1 of Chen et al. (2019) to directly estimate parameter values or place limits on them.

Figure 2 displays our line profile fits for all C IV doublets included in the final catalog. The velocity shift v , covering fraction C_0 , and column density $\log N$ are derived from Equations (1) to (3) through fitting the C IV doublet line profiles. Figure 3, Figure 4, Figure 5 and

Figure 6 illustrate the fitted profiles for the Si IV, N V, O VI, and Lyman AALs, respectively, as included in the final catalog.

3.2. Line-locked Signatures

We searched for line-locked pairs of absorption lines corresponding to the C IV, Si IV, O VI, and N V doublets in the quasar J151352+085555 spectrum, utilizing the component matrix in velocity space displayed in Figure 7. Line-locked pairs can be identified within the matrix by drawing a straight line with a slope of +1, with the intercept corresponding to the doublet velocity separation, which is approximately 498 km s⁻¹ for C IV, 964 km s⁻¹ for N V, 1939 km s⁻¹ for Si IV, and 1650 km s⁻¹ for O VI.

We define two absorbers as line-locked if their velocity difference meets the criterion:

$$|\delta v - v_{\text{sep}}| \leq \min(b_1, b_2, 0.1 \times v_{\text{sep}}), \quad (4)$$

where v_{sep} represents the velocity separation of the doublet, and b_1 and b_2 are the Doppler parameters of the two lines, respectively. Confirmed line-locked pairs are indicated using colored brackets in Figures 2 to 5.

In Figure 2, two line-locked pairs of C IV absorbers are identified: pairs (5, 7) and (8, 11), with separations matching the C IV $\lambda 1548, 1551$ doublet. We also detect line-locking among other ionic doublets, including Si IV $\lambda 1393, 1403$, N V $\lambda 1239, 1243$, and O VI $\lambda 1032, 1038$. For Si IV, two line-locked groups are found: (3, 6, 10) and (5, 9), as marked in red in Figure 3. In the case of N V, three successive doublets (3, 4, 6) form a line-locked complex, highlighted in Figure 4. We also identify three line-locked pairs in the O VI doublet: (1, 3, 5), (6, 9), and (7, 10).

The line-locking web can manifests as velocity-stabilized absorption features in quasar spectra, caused by the combined effects of multiple line-locking processes involving ions like C IV, N V, Si IV, and O VI, etc. Clouds in the web show distinct velocity separations matching the doublet spacings of common UV resonance transitions. From the component matrix in Figure 7, we have identified one of the largest line-locking web known to date. This web contains ten absorbers, which are interconnected through doublets of C IV, Si IV, N V, and O VI. Its structure is illustrated in the schematic shown in Figure 8. Such web configuration could occur by chance, we estimated the probability of alignment by chance following the approach of Srianand et al. (2002). We randomly populated 12 absorbers within the velocity space of -7000 to 0 km/s. The probability of detecting the arrangement depicted in Figure 8 is found to be $< 10^{-8}$. This low chance alignment probability, together with the

observation of multiple line-locked doublets in the same quasar (e.g., Ganguly & Brotherton 2008; Hamann et al. 2011), supports line-locking as a natural consequence of radiative acceleration (Srianand et al. 2002; Juráňová et al. 2024). Traditionally, theoretical studies of line-locking have often employed simplified two-cloud models to explore the phenomenon (Lewis & Chelouche 2023). The identification of the largest line-locking web calls for more sophisticated modeling. Potential interactions among the line-locked clouds in the web presents an interesting research topic for the future.

3.3. Photoionization model

In this section, we explore the physical conditions of the absorber systems based on photoionization modeling. To gain insights into the ionization states, total column density, and element abundances of the absorbers, we employed the CLOUDY 2023 release (Chatzikos et al. 2023). Although a specific ionic column density can arise under various physical conditions, combining constraints from multiple ionic species helps narrow down the range of possible gas properties in the absorption systems. All 12 narrow absorption line (NAL) components identified (components 1 to 12) in Section 3.2 have measured column densities for at least two ion species, as listed in Table 1.

We run CLOUDY using a generic fixed H I column density of $\log N(\text{H I})(\text{cm}^{-2}) = 15$ that ensures that the clouds are optically thin in the Lyman continuum. This is justified by the measurements and upper limits on $N(\text{H I})$ that we derive from the data (Table 1). In this optically thin regime, the column density ratios needed for our analysis do not depend on $N(\text{H I})$ nor $N(\text{H})$. The calculations assume solar abundances and a standard quasar ionizing spectrum.

The ionization state of the absorbers is described by the ionization parameter, U , which is the dimensionless ratio of the number density of hydrogen-ionizing photons at the illuminated face of the clouds to the number density of hydrogen atoms. Figure 9 shows the calculated ionization fractions in important ions compared to well-measured column density ratios in the data (e.g., Si IV/C IV, C IV/N V, N V/O VI, etc.). These comparisons yield estimates of the ionization parameter U (shown by the orange vertical lines in the figure) with uncertainties (orange shadows) based on the column density uncertainties listed in the data tables (see Section 4.3 in Chen et al. (2018) and Section 4.1.1 in Chen et al. (2019) for more details). In particular, if a component exhibiting absorption lines for multiple ions (e.g. Si IV, C IV, N V); in that case, the ion ratios (e.g. Si IV/C IV, C IV/N V, N V/Si IV) can yield distinct U val-

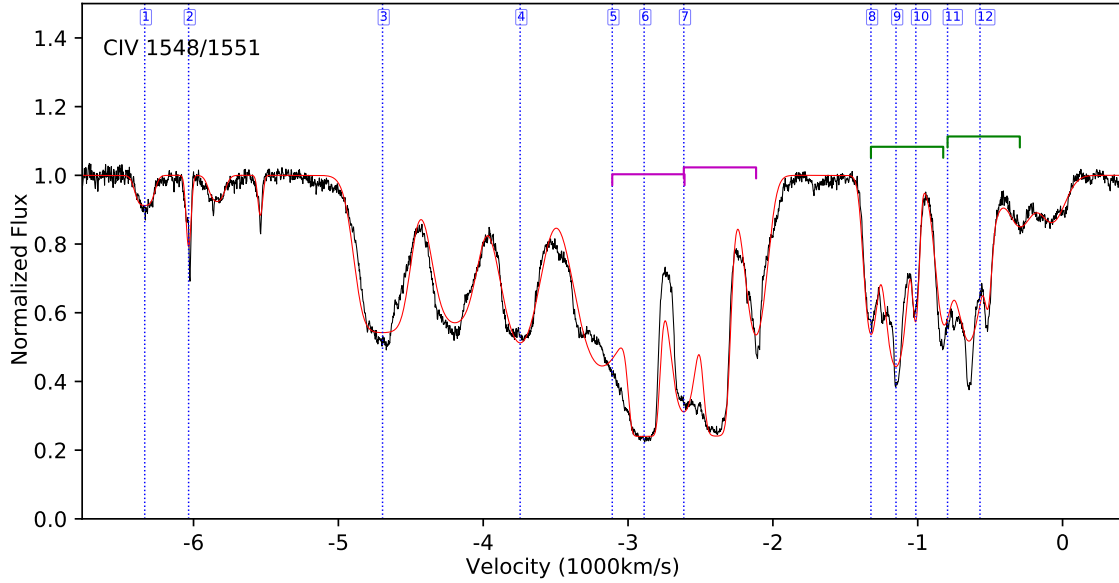


Figure 2. Normalized CIV line profiles in the VLT-UVES spectra plotted on a velocity scale relative to the quasar redshift $z = 2.901$. The spectra are shown in black, and the final fitting lines are shown in red. The blue dash lines are identified components from 1 to 12, and the brackets show the line-locked doublets. The velocities pertain to the short-wavelength lines in the doublets.

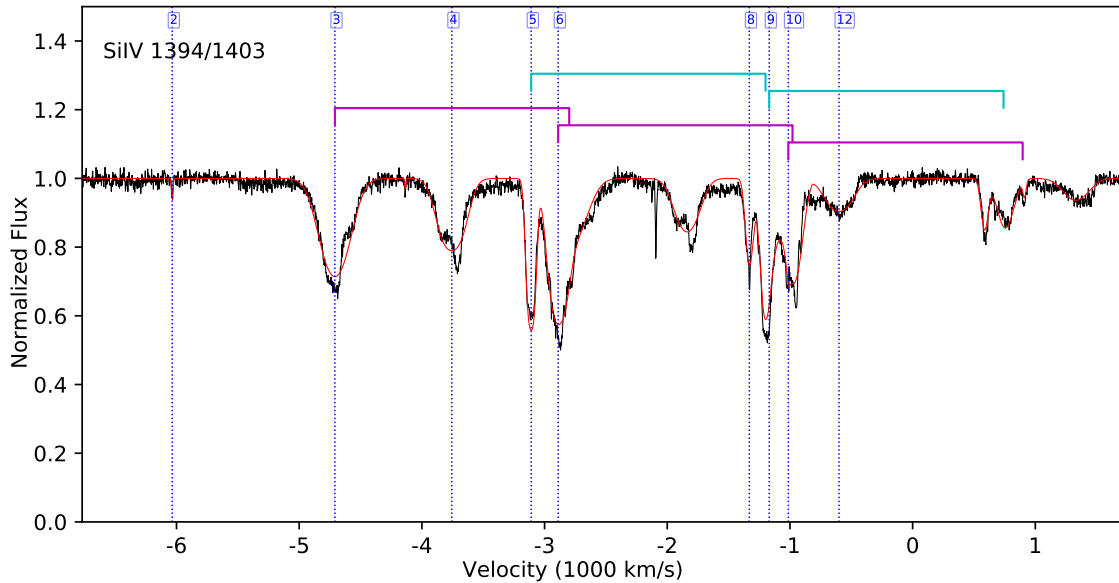


Figure 3. Normalized SiIV line profiles in the VLT-UVES spectra plotted on a velocity scale relative to the quasar redshift $z = 2.901$. The spectra are shown in black, and the final fitting lines are shown in red. The blue dash lines are identified components, and the brackets show the line-locked doublets. The velocities pertain to the short-wavelength lines in the doublets.

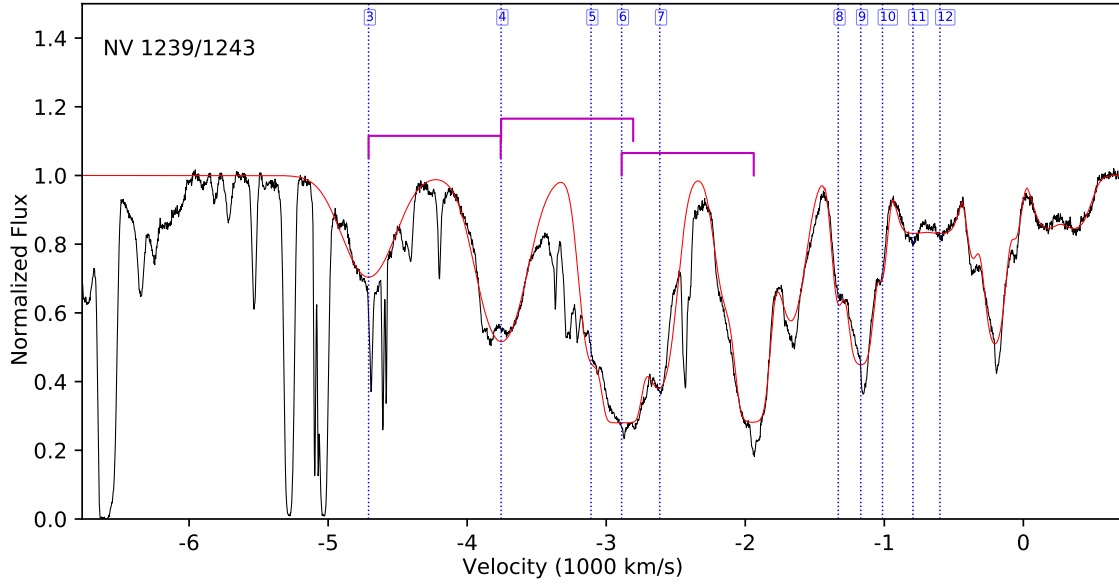


Figure 4. Normalized NV line profiles in the VLT-UVES spectra plotted on a velocity scale relative to the quasar redshift $z = 2.901$. The spectra are shown in black, and the final fitting lines are shown in red. The blue dash lines are identified components, and the brackets show the line-locked doublets. The velocities pertain to the short-wavelength lines in the doublets.

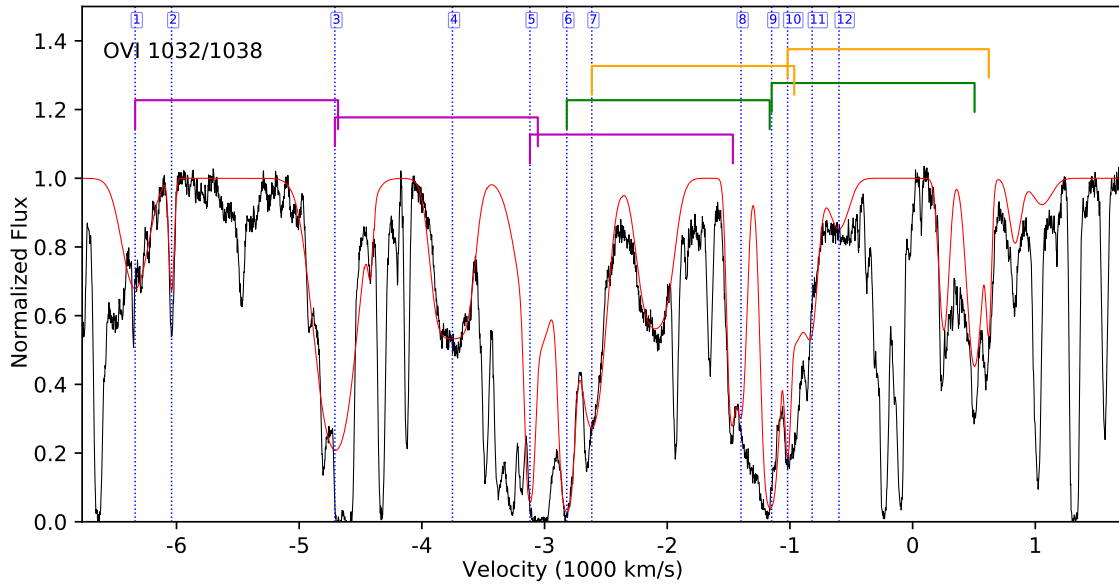


Figure 5. Normalized OVI line profiles in the VLT-UVES spectra plotted on a velocity scale relative to the quasar redshift $z = 2.901$. The spectra are shown in black, and the final fitting lines are shown in red. The blue dash lines are identified components, and the brackets show the line-locked doublets. The velocities pertain to the short-wavelength lines in the doublets.

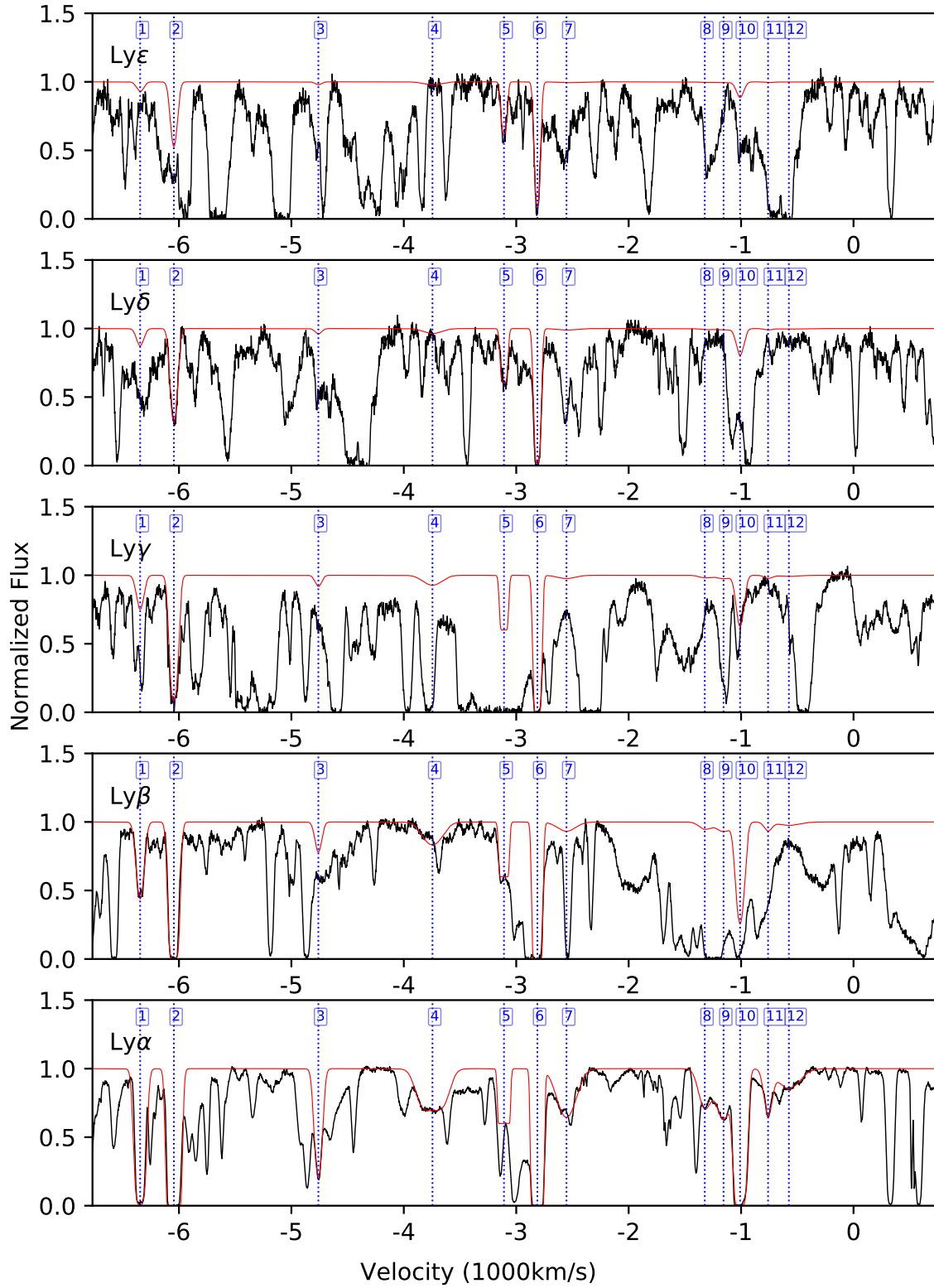


Figure 6. Normalized Lyman line profiles in the VLT-UVES spectra plotted on a velocity scale relative to the quasar redshift $z = 2.901$. The spectra are shown in black, and the final fitting lines are shown in red. The blue dash lines are identified components from 1 to 12, and the brackets show the line-locked doublets. The velocities pertain to the short-wavelength lines in the doublets.

Table 1. Individual absorption lines of J151352+085555. Columns show component number, absorption redshift (z_{abs}) and the corresponding velocity shift (v) relative to the emission-line redshift 2.901 (Murphy et al. 2019), line identification and rest wavelength, observation wavelength, Doppler b parameter, logarithm of column density, covering fraction, and notes ('bl'=blended with neighboring systems or unrelated lines, if the blended system is also measured, we record bl-X to indicate the component number of the other system).

#	z_{abs}	v (km s ⁻¹)	ID1	λ_{obs1} (Å)	ID2	λ_{obs2} (Å)	b (km s ⁻¹)	$\log N$ (cm ⁻²)	C_0	Notes
1	2.8186	-6337		Lyman Series			44.0 ± 1.2	14.48 ± 0.01	1.0	
			O VI 1032	3940.51	O VI 1038	3962.24	129.6 ± 10.3	$\gtrsim 14.40$	$0.33 \sim 1.0$	bl,bl-3
			C IV 1548	5911.94	C IV 1551	5921.77	54.4 ± 2.0	14.66 ± 0.06	0.09 ± 0.01	
2	2.8226	-6029		Lyman Series			39.3 ± 0.7	15.36 ± 0.01	1.0	
			O VI 1032	3944.64	O VI 1038	3966.39	26.4 ± 1.0	14.25 ± 0.08	0.58 ± 0.07	
			Si IV 1394	5327.94	Si IV 1403	5362.23	7.8 ± 7.5	11.64 ± 0.36	1.0	weak line
3	2.8398	-4706		Lyman Series			22.8 ± 1.3	13.41 ± 0.31	0.53 ± 0.32	
			O VI 1032	3962.39	O VI 1038	3984.24	39.7 ± 0.9	$\gtrsim 13.91$	$0.83 \sim 1.0$	
			N V 1239	4756.82	N V 1243	4772.12	214.2 ± 18.9	$\gtrsim 15.15$	≤ 1.0	bl,bl-1,5
4	2.8522	-3753		Lyman Series			240.0 ± 18.9	14.64 ± 0.03	0.72 ± 0.05	bl,bl-4
			Si IV 1394	5351.91	Si IV 1403	5386.36	153.5 ± 37.2	14.12 ± 0.11	0.45 ± 0.08	bl-6
			C IV 1548	5944.76	C IV 1551	5954.65	140.9 ± 1.6	15.24 ± 0.02	0.46 ± 0.01	
5	2.8606	-3107		Lyman Series			111.4 ± 2.5	14.85 ± 0.02	0.31 ± 0.01	bl
			O VI 1032	3975.19	O VI 1038	3997.11	130.7 ± 2.7	15.54 ± 0.03	0.47 ± 0.01	
			N V 1239	4772.19	N V 1243	4787.53	197.9 ± 6.1	14.76 ± 0.10	0.46 ± 0.19	bl-3,5,6,7
6	2.8635	-2884		Lyman Series			120.8 ± 3.0	14.37 ± 0.04	0.24 ± 0.02	
			Si IV 1394	5369.20	Si IV 1403	5403.75	120.8 ± 3.0	14.37 ± 0.04	0.24 ± 0.02	
			C IV 1548	5963.96	C IV 1551	5973.88	164.5 ± 1.7	14.58 ± 0.05	0.57 ± 0.08	bl-5
7	2.8671	-2607		Lyman Series			25.8 ± 3.0	$\lesssim 15.87$	$0.40 \sim 1.0$	bl
			O VI 1032	3983.85	O VI 1038	4005.82	51.8 ± 0.9	$\gtrsim 14.77$	≤ 1.0	bl,bl-3
			N V 1239	4782.59	N V 1243	4797.97	95.2 ± 27.8	14.64 ± 0.11	0.66 ± 0.08	bl-4,6,7
8	2.8838	-1323		Lyman Series			39.1 ± 11.9	14.00 ± 0.24	0.41 ± 0.09	bl-9
			Si IV 1394	5380.90	Si IV 1403	5415.53	39.1 ± 11.9	14.00 ± 0.24	0.41 ± 0.09	
			C IV 1548	5976.96	C IV 1551	5986.90	240.5 ± 26.5	14.72 ± 0.21	0.50 ± 0.08	bl-4,6,7
9	2.8859	-1161		Lyman Series			27.8 ± 0.6	15.78 ± 0.01	1.0	
			O VI 1032	3986.85	O VI 1038	4008.83	60.1 ± 2.3	14.99 ± 0.03	1.0	bl-9
			N V 1239	4786.18	N V 1243	4801.57	96.1 ± 10.8	15.61 ± 0.13	0.59 ± 0.04	bl-4,5,7
10	2.8879	-1007		Lyman Series			84.6 ± 20.8	14.21 ± 0.13	0.41 ± 0.07	bl-3,10
			Si IV 1394	5384.95	Si IV 1403	5419.60	84.6 ± 20.8	14.21 ± 0.13	0.41 ± 0.07	
			C IV 1548	5981.45	C IV 1551	5991.40	67.7 ± 1.8	15.30 ± 0.04	0.78 ± 0.05	bl-5,7
11	2.8908	-784		Lyman Series			111.7 ± 3.6	$\gtrsim 13.81$	$0.43 \sim 1.0$	bl
			O VI 1032	3990.56	O VI 1038	4012.57	126.8 ± 2.5	$\gtrsim 14.90$	$0.75 \sim 1.0$	bl-10
			N V 1239	4790.64	N V 1243	4806.05	120.9 ± 1.8	14.87 ± 0.04	0.67 ± 0.06	bl-4,5,6
12	2.8933	-592		Lyman Series			89.7 ± 1.5	14.58 ± 0.05	0.67 ± 0.07	bl-5,6
			C IV 1548	5987.02	C IV 1551	5996.98	89.7 ± 1.5	14.58 ± 0.05	0.67 ± 0.07	
			O VI 1032	4007.79	O VI 1038	4029.90	72.3 ± 3.8	$\gtrsim 13.51$	$0.31 \sim 1.0$	bl
13	2.8933	-592		Lyman Series			52.6 ± 2.1	$\gtrsim 14.48$	$0.75 \sim 1.0$	bl,bl-5,9
			N V 1239	4811.33	N V 1243	4826.80	55.6 ± 1.7	14.30 ± 0.10	0.48 ± 0.12	bl-9,10
			Si IV 1394	5413.24	Si IV 1403	5448.08	38.6 ± 1.4	13.42 ± 0.17	0.46 ± 0.18	
14	2.8933	-592		Lyman Series			56.1 ± 5.5	14.19 ± 0.11	0.59 ± 0.11	bl-11
			C IV 1548	6012.88	C IV 1551	6022.88	56.1 ± 5.5	14.19 ± 0.11	0.59 ± 0.11	
			O VI 1032	4009.96	O VI 1038	4032.07	87.2 ± 1.3	$\gtrsim 13.73$	$0.39 \sim 1.0$	bl
15	2.8933	-592		Lyman Series			76.0 ± 2.9	$\gtrsim 14.77$	$0.90 \sim 1.0$	bl,bl-6,10
			N V 1239	4813.93	N V 1243	4829.41	80.8 ± 1.5	15.06 ± 0.02	0.55 ± 0.05	bl-8,10
			Si IV 1394	5416.17	Si IV 1403	5451.02	90.1 ± 43.3	13.78 ± 0.19	0.40 ± 0.13	bl-5
16	2.8933	-592		Lyman Series			83.0 ± 8.1	14.56 ± 0.17	0.59 ± 0.07	bl-11,12
			C IV 1548	6016.13	C IV 1551	6026.14	83.0 ± 8.1	14.56 ± 0.17	0.59 ± 0.07	
			O VI 1032	4012.03	O VI 1038	4034.15	29.0 ± 4.0	$\gtrsim 14.18$	$0.84 \sim 1.0$	bl,bl-7,9,11
17	2.8933	-592		Lyman Series			45.2 ± 4.2	14.70 ± 0.03	1.0	bl
			O VI 1032	4012.03	O VI 1038	4034.15	29.0 ± 4.0	$\gtrsim 14.18$	$0.84 \sim 1.0$	bl,bl-7,9,11
			N V 1239	4816.41	N V 1243	4831.90	46.8 ± 2.1	14.03 ± 0.12	0.47 ± 0.18	bl-9
18	2.8933	-592		Lyman Series			18.0 ± 13.2	12.56 ± 0.57	0.46 ± 0.48	bl-6
			Si IV 1394	5418.96	Si IV 1403	5453.83	18.0 ± 13.2	12.56 ± 0.57	0.46 ± 0.48	
			C IV 1548	6019.23	C IV 1551	6029.24	28.6 ± 3.4	13.78 ± 0.12	0.56 ± 0.18	bl-12
19	2.8933	-592		Lyman Series			47.4 ± 1.3	$\gtrsim 13.41$	$0.36 \sim 1.0$	bl
			O VI 1032	4015.02	O VI 1038	4037.16	64.1 ± 6.9	$\gtrsim 14.12$	≤ 1.0	bl,bl-7,10,12
			N V 1239	4820.00	N V 1243	4835.50	93.3 ± 2.1	15.16 ± 0.02	0.13 ± 0.05	bl-12
20	2.8933	-592		Lyman Series			109.7 ± 4.0	14.10 ± 0.15	0.56 ± 0.16	bl-8,9
			C IV 1548	6023.72	C IV 1551	6033.74	109.7 ± 4.0	14.10 ± 0.15	0.56 ± 0.16	
			O VI 1032	4017.60	O VI 1038	4039.75	-	$\gtrsim 13.44$	$0.26 \sim 1.0$	bl
21	2.8933	-592		Lyman Series			-	-	≤ 1.0	bl,bl-11
			O VI 1032	4017.60	O VI 1038	4039.75	-	-	≤ 1.0	bl,bl-11
			N V 1239	4823.10	N V 1243	4838.61	107.6 ± 2.1	15.24 ± 0.02	0.14 ± 0.04	bl-11
22	2.8933	-592		Lyman Series			129.9 ± 3.9	14.21 ± 0.06	0.13 ± 0.01	
			Si IV 1394	5426.48	Si IV 1403	5461.40	129.9 ± 3.9	14.21 ± 0.06	0.13 ± 0.01	
			C IV 1548	6027.59	C IV 1551	6037.61	117.6 ± 9.7	14.10 ± 0.15	0.52 ± 0.17	bl-9,10

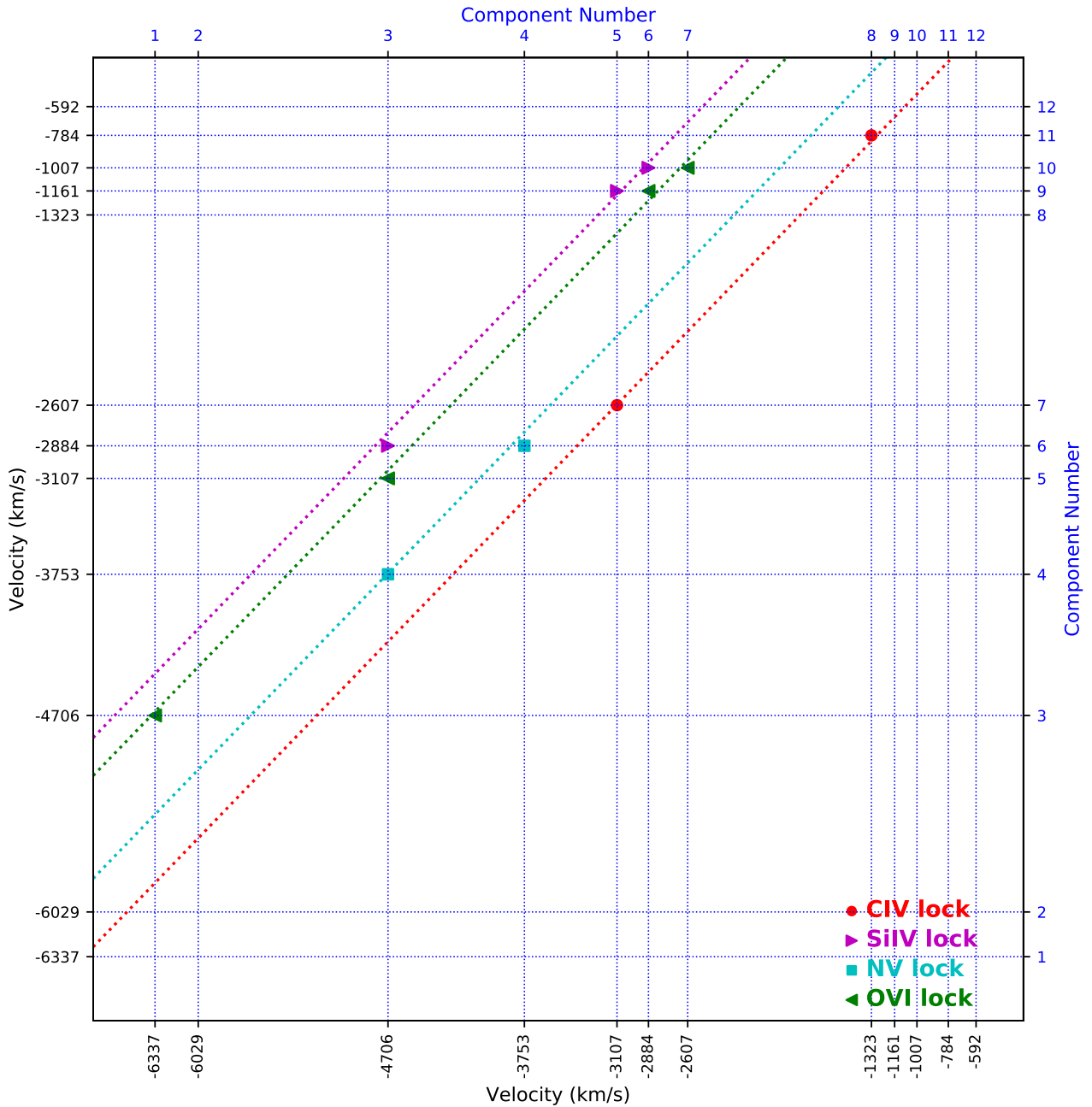


Figure 7. The component matrix shows all possible line locks in C IV, Si IV, N V and O VI based on their velocity separations. We consider two systems locked when their velocity separation is a close match (with errors less than 10%) to their laboratory doublet separation (see text for details). All line-locking pairs corresponding to the same ion doublet sit on the same line, where red line for C IV doublet, purple line for Si IV, cyan line for N V, and green line for O VI.

ues. We derive a weighted mean (based on column densities uncertainties) to be the best U value and a weighted error to be the measurement error.

Subsequently, we derive the total hydrogen column density, $N(\text{H})$, for components 2, 4, 6 and 10 that have well-measured $N(\text{H I})$ values, and estimate upper or lower limits on $N(\text{H})$ for other components with only upper or lower limits on $N(\text{H I})$. This is accomplished by applying an ionization correction, $\text{H I}/\text{H}$, appropriate for

the derived U values to the $N(\text{H I})$ values measured from the data. The results are shown in Figure 10. The derived values span ranges of $\log N(\text{H})$ (cm^{-2}) from ~ 18 to ~ 20.5 and $\log U$ from ~ -1 to ~ 0 , consistent with the findings of Srianand et al. (2002). In that study, the physical conditions of a single component (component e, corresponding to our component 5) were explored, yielding $-2.0 \leq \log U \leq -0.6$ and $10^{19} \text{ cm}^{-2} \leq N(\text{H}) \leq 10^{20}$

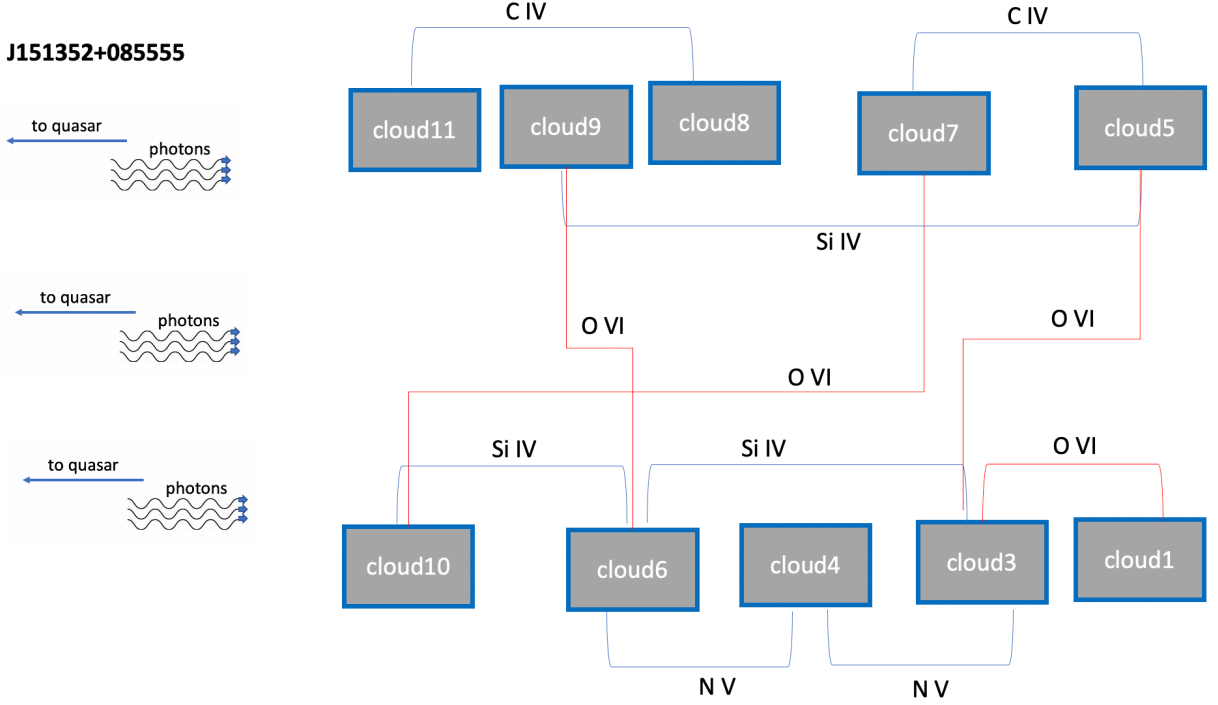


Figure 8. The complex absorber systems line-locked through multi-ion doublets detected in the spectrum of J151352+085555. All absorbers are exposed to ionizing radiation coming from the quasar on the left. The number inside the cloud box is the corresponding component index shown in Table 1. We also show if the cloud having C IV, Si IV, N V and O VI doublets identified.

cm^{-2} , in agreement with our results of $\log U \sim -0.9$ and $N(\text{H}) \lesssim 10^{20.3} \text{ cm}^{-2}$.

We then estimate the component metallicities using the general relation (see more details in [Chen et al. 2018, 2019](#)):

$$\left[\frac{\text{M}}{\text{H}} \right] = \log \left(\frac{N(\text{M}_i)}{N(\text{H I})} \right) + \log \left(\frac{f(\text{H I})}{f(\text{M}_i)} \right) + \log \left(\frac{\text{H}}{\text{M}} \right)_{\odot}, \quad (5)$$

where $(\text{H}/\text{M})_{\odot}$ is the solar abundance ratio of hydrogen to some metal M, $N(\text{H I})$ and $f(\text{H I})$ are the column density and ionization fraction of H I, respectively, and $N(\text{M}_i)$ and $f(\text{M}_i)$ are the column density and ionization fraction of ion M_i of metal M, respectively. In particular, $N(\text{M}_i)$ and $N(\text{H I})$ are derived from our fitting process. We use our estimates of U to determine the ionization correction factor $f(\text{H I})/f(\text{M}_i)$ from the CLOUDY calculations, and then plug in measured values of the column densities to obtain the metal abundance $[\text{M}/\text{H}]$.

The results for $[\text{Si}/\text{H}]$, $[\text{C}/\text{H}]$, $[\text{N}/\text{H}]$ and/or $[\text{O}/\text{H}]$, depending on lines available, are shown in Figure 11. The error bars shown in this figure are derive only from the measurement uncertainties in the corresponding ion col-

umn densities. Figure 11 shows a mixture of metallicity results for the five components. We have metallicity estimates for components 2, 4, 5, 6, and 10 because their H I column densities have been accurately measured or an upper limit has been estimated. For the other components, we have not displayed the limits because the lower limits on $N(\text{H I})$ result in high upper bounds for metallicity, well above solar, which do not offer meaningful constraints for our analysis.

Component 2 shows substantially sub-solar metallicity, very high velocity, and a sharp line profile, which are very different from the other 10 locked components. This indicates component 2 may form in a physically distinct region compared to the other locked components, likely farther away from the background continuum source—perhaps in the halo. This difference could explain why it is not locked with the other components. In components 6, we also find evidence for enhanced nitrogen abundance, with $[\text{N}/\text{C}] > 0$, as reported in the literature ([Petitjean et al. 1994, 2008](#); [Fechner & Richter 2009](#)). For example, [Fechner & Richter \(2009\)](#) find 27% of the associated systems show clearly enhanced nitrogen. In Paper I, we also obtained reasonable $[\text{N}/\text{C}]$ value

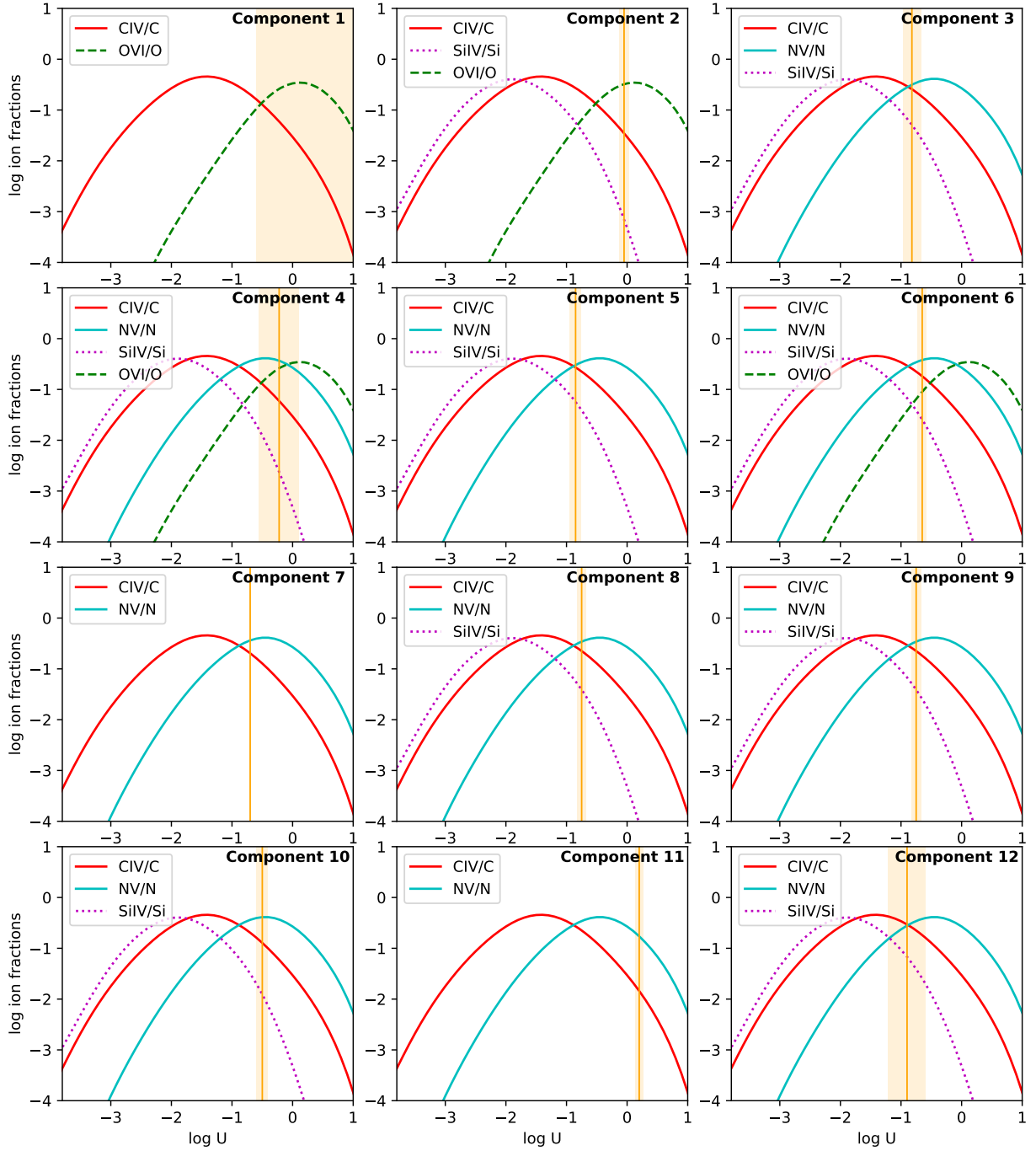


Figure 9. Theoretical ionization fractions, $f(M_i)$, for selected stages of the elements Si, C, N and O plotted against ionization parameters $\log U$. The orange vertical lines with orange shadows are the best estimations and errors of U for each component.

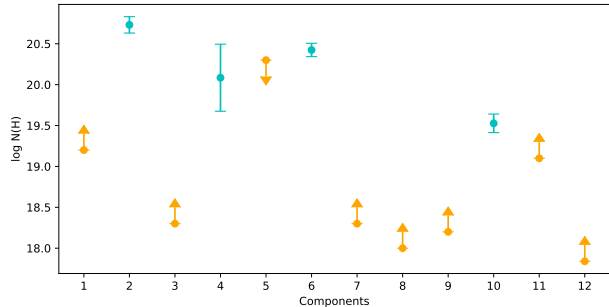


Figure 10. Total hydrogen column density $\log N(\text{H})$ for components 1-12. The orange and cyan color codes correspond to the upper or lower limits and the well-measured column densities, respectively.

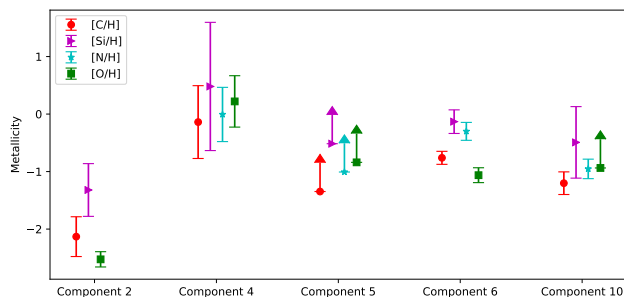


Figure 11. C, Si, N, O abundances for components 2, 4, 5, 6 and 10.

for component 9 in Quasar J221531-174408. Using data from this study (component 4, 5, 6, 10) and Paper I (component 9), we find 20% (1 out of 5) NALs show evidence of enhanced nitrogen. Due to the small sample size of 5, this result should be considered preliminary and warrants further investigation with larger datasets to confirm its validity.

Assuming a tenth solar metallicity, cloud sizes ranging from 0.1 to 1 pc, and hydrogen column densities of $\log N(\text{H})(\text{cm}^{-2})$ ranging from 18 to 20.5 as derived from CLOUDY, we estimate the masses of typical absorbers to lie between 1×10^{-4} and $3 M_{\odot}$. Following the method of Paper I, we also estimate the total kinetic energy of the outflow system identified through line-locking, and evaluate its impact on the host galaxy’s evolution from the energetic perspective. Assuming typical distances of ~ 10 – 100 pc for the line-locking clouds, we obtain kinetic energies $K \lesssim 1.65 - 165 \times 10^{53}$ ergs, and total kinetic luminosity of $\dot{K} \lesssim (0.2 - 2) \times 10^{43}$ ergs s^{-1} for this line-locking web. The resulting ratios between the kinetic energy rate and bolometric luminosity, $\dot{K}/L_{\text{Bol}} \lesssim (0.5 - 5) \times 10^{-5}$, is two orders of magnitude lower than the threshold of 0.005 to 0.05 required for effective feedback to the host galaxies (Scannapieco & Oh 2004; Di

Matteo et al. 2005; Prochaska & Hennawi 2009; Hopkins & Elvis 2010). The conclusion is that the kinetic luminosity of the NAL outflow system is quite low compared to the bolometric luminosity of the quasar, which is consistent with the findings for the NAL outflow system in Quasar J221531-174408, as reported in our Paper I.

4. DISCUSSION

4.1. Comparison with Previous Studies

Quasar J151352+085555 is one of only four known quasars exhibiting line-locking (LL) signatures in at least C IV, Si IV, and N V doublets simultaneously. The other three are Q1303+308 (Turnshek et al. 1984; Foltz et al. 1987; Braun & Milgrom 1989), J221531-174408 (Chen et al. 2024), and SDSS J092345+512710 (Lin & Lu 2020b). As illustrated in Figure 8, quasar J151352+085555 exhibits one of the most complex LL structures reported in the literature. Ten out of the twelve identified NAL absorbers are linked through radiative forces, as evidenced by their velocity separations corresponding to the C IV, Si IV, O VI, and N V doublets. As discussed in Section 2, Srianand et al. (2002) is the first to identify the LL phenomena in quasar J151352+085555. They have investigated its LL properties using the UVES observation obtained at year 2000. Our analysis here uses the combined data obtained from UVES observation at year 2000, 2002, and 2003, and reveals some differences compared to the findings of Srianand et al. (2002).

While Srianand et al. (2002) focused on LL signatures associated with the O VI, N V, and C IV doublet splittings, we also identify two additional LL pairs corresponding to Si IV. Both studies have detected two pairs of LLs in C IV; however, we identify one different pair compared to their results. The first C IV LL pair reported by Srianand et al. (2002) (the b-c pair) is considered marginal in our analysis due to poor matching between the line profiles of the two components. The detected N V LL pairs are consistent between both works. Our study find two double LL pairs and one triple LL pair in O VI, while Srianand et al. (2002) detected only one triple LL pair. The discrepancies arise mainly from differences in data reduction methods and LL identification technique. Specifically, we have identified seven additional LL pairs compared to Srianand et al. (2002), thanks to the improved data reduction provided by Murphy et al. (2019) and the use of a different LL signature identification algorithm.

Srianand et al. (2002) have studied physical parameters of component e (corresponding to component 5 in this study) using a photoionization model. They reported a covering fraction of 0.4 and column density

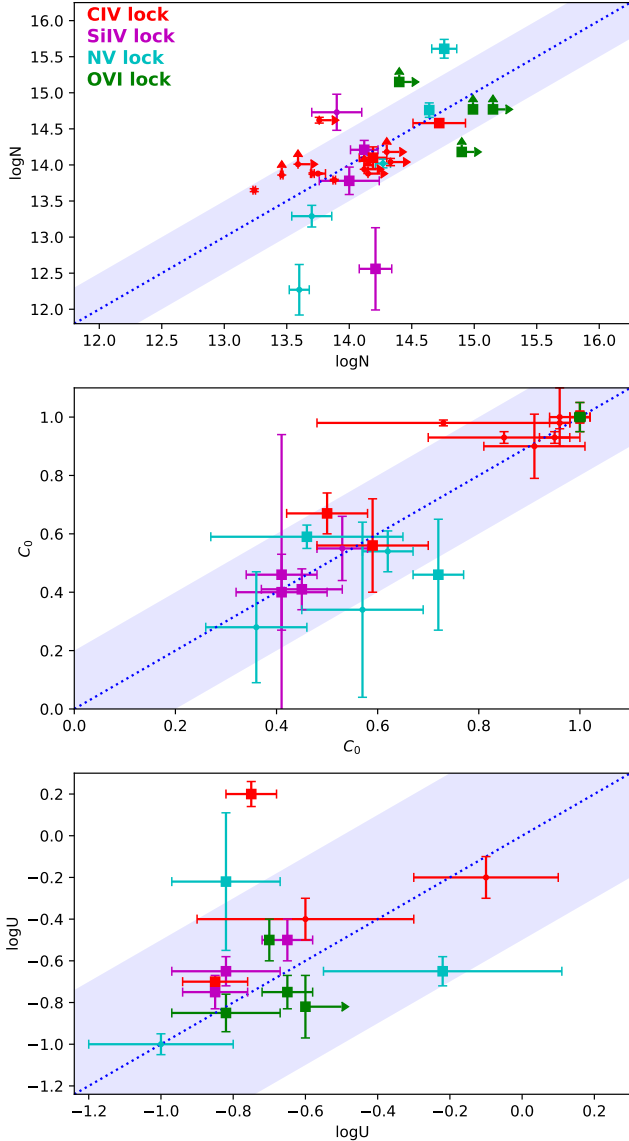


Figure 12. Comparison between the derived properties of the shadowed cloud (X-axis) and shadowing cloud (Y-axis) in the same line-lock pair. Upper panel: logarithm of column density. Middle panel: covering fraction. Lower panel: logarithm of ionization. The blue dashed line indicates a 1:1 ratio. In the upper and lower panels, the blue shadows delineate the region where the parameters of the shadowing clouds are within a factor of ~ 3 above and below those of the shadowed clouds. In the middle panel, the blue shadow marks the 20% uncertainty area around the 1:1 ratio line. The sample contains all the line-locked systems that were analyzed in Chen et al. (2018, 2019, 2024) (represented by filled dot symbols) and this paper (represented by the filled square symbols).

$\log N(HI)$ around 16.3, while we obtained values of $\gtrsim 0.4$ and $\lesssim 15.8$, respectively. They have shown the ionization parameter of component 5 should be in the range $-2.0 < \log U < -0.6$, while we gave a value around -0.9. For the total hydrogen column density of component 5, Srianand et al. (2002) gave $19 \lesssim \log N(H) \lesssim 20$, and we obtained a value of $\log N(H) \lesssim 20.3$. For all the other components presented in their Table 1, the covering fractions generally agree with results presented in our Table 1. In Srianand et al. (2002) they argued the distance of the absorbers to the background continuum source is between 0.1 pc to a few kpc, while we simply adopted typical values of 10-100 pc when estimating the total gas mass in the outflow in Section 3.3. We also placed constraints on the metallicities of five components to be equal to or less than solar, whereas Srianand et al. (2002) did not report any metallicity measurements. The above comparisons focusing on component 5 suggest both studies yielded similar line fitting and ionization results. And we can conclude that the main differences between the two studies are the LL structure identified, possibly due to different LL identification technique.

4.2. ‘Shadowed’ vs ‘Shadowing’ absorbers

We find ten out of the twelve NALs identified in the J151352+085555 spectra appear line-locked, which represents a notably high percentage. This suggests that line-locking may be prevalent in quasar outflow, like suggested by Bowler et al. (2014), and Chen et al. (2021a). Although the specific physical mechanism is still under debate (see the discussion in Bowler et al. 2014), it is widely agreed that line-locked systems are related to the physical process of radiative acceleration (Milne 1926; Scargle 1973; Braun & Milgrom 1989; Lewis & Chelouche 2023; Dannen et al. 2024), where successive shielding of the outflowing clouds locks the clouds one by one in outflow velocity. Using simulations, Lewis & Chelouche (2023) suggests the clouds’ properties need to be fine-tuned to within 1% for the clouds to be line-locked. The case presented here, together with our previously studied cases (Chen et al. 2018, 2019, 2024), can be used for a preliminary statistical test of this scenario. We have compared the ion column density, coverage fraction, and $\log U$ between the ‘shadowed’ absorbers and ‘shadowing’ absorbers in Figure 12. We find that most ion column densities and ionization parameters of the shadowing clouds lie within a factor of ~ 3 of those of the shadowed clouds. Additionally, the coverage fractions of the shadowing clouds are comparable to those of the shadowed clouds. This generally supports the study of Lewis & Chelouche (2023), where they argue the two

absorbers need to have similar physical properties. However, we also find exceptions, suggesting that clouds with quite different physical conditions can also be locked together, and fine-tuning is not always required.

One possible solution to the discrepancies between observational evidence and the theoretical prediction of Lewis & Chelouche (2023) is to add more clouds (> 10) and multi-ionic LL (> 3) to the modeling process, instead of using a simple two clouds one doublet model. Further theoretical modeling and detailed simulations are needed to reveal the mechanisms behind these line-locking phenomena.

5. CONCLUSION

As the second paper in a series of TOLL project, we have conducted a detailed investigation of line-locking signatures in QSO J151352+085555 using high-resolution, high signal-to-noise ratio archived VLT-UVES spectra. Our study provides a significant improvement in sensitivity to weak and narrow associated absorption lines compared to previous outflow line-locking surveys conducted with medium-resolution spectra, such as those from the SDSS. A total of 12 associated absorption line systems were identified, and we performed detailed fitting for each C IV, N V, Si IV, and O VI narrow absorption line to derive physical properties, including velocity shifts, column densities, and line-of-sight covering fractions, C_0 . We find that these AALs have covering fractions ranging from ~ 0.4 to ~ 1 , and $\log U$ values ranging from -1.0 to 0.0 . Ten out of the 12 identified AALs exhibit line-locking signatures, forming one of the largest line-locking web known to date. Dis-

covery of this line-locking web calls for more sophisticated theoretical model and simulation works to explain its formation and evolution.

We have also compared the properties of the shadowed and shadowing cloud in the same line-locking pair, using data from our previous works and this study. We find they tend to have similar $\log N$, $\log U$, and C_0 values, with a few exceptions. Our findings suggest that it is necessary to use high-resolution, high-SNR spectra to study the line-locking phenomena in quasar outflow. The data presented in this paper can be used to test theoretical models in the future.

ACKNOWLEDGMENTS

We want to extend our heartfelt gratitude to Prof. Fred Hamann, now retired, for initiating this project and for his invaluable guidance as the PhD advisor of Dr. Chen Chen. To enjoy a peaceful retirement life, Prof. Fred Hamann has opted to remove his name from the co-author list. His mentorship and expertise have been instrumental in shaping the direction of this project. We wish him a happy and healthy retirement. We also thank Prof. Michael Murphy for providing the quasar spectrum. This work was supported in part by the National Natural Science Foundation of China (12103097, 12073092), the National Key R&D Program of China (2020YFC2201400). CC acknowledges the support of the ‘Three Levels’ Talent Construction Project of Zhuhai College of Science and Technology. Z. C. He acknowledges the support of the National Natural Science Foundation of China (Grant Nos. 12222304, 12192220, and 12192221).

REFERENCES

- Abolfathi, B., Aguado, D. S., Aguilar, G., et al. 2018, *ApJS*, 235, 42, doi: [10.3847/1538-4365/aa9e8a](https://doi.org/10.3847/1538-4365/aa9e8a)
- Anderson, S. F., Weymann, R. J., Foltz, C. B., & Chaffee, Frederic H., J. 1987, *AJ*, 94, 278, doi: [10.1086/114468](https://doi.org/10.1086/114468)
- Anglés-Alcázar, D., Davé, R., Faucher-Giguère, C.-A., Özel, F., & Hopkins, P. F. 2017a, *MNRAS*, 464, 2840, doi: [10.1093/mnras/stw2565](https://doi.org/10.1093/mnras/stw2565)
- Anglés-Alcázar, D., Faucher-Giguère, C.-A., Quataert, E., et al. 2017b, *MNRAS*, 472, L109, doi: [10.1093/mnrasl/slx161](https://doi.org/10.1093/mnrasl/slx161)
- Arav, N. 1996, *ApJ*, 465, 617, doi: [10.1086/177447](https://doi.org/10.1086/177447)
- Arav, N., & Begelman, M. C. 1994, *ApJ*, 434, 479, doi: [10.1086/174748](https://doi.org/10.1086/174748)
- Arav, N., Korista, K. T., Barlow, T. A., & Begelman. 1995, *Nature*, 376, 576, doi: [10.1038/376576a0](https://doi.org/10.1038/376576a0)
- Arav, N., Li, Z.-Y., & Begelman, M. C. 1994, *ApJ*, 432, 62
- Ayubinia, A., Woo, J.-H., Rakshit, S., & Son, D. 2023, *ApJ*, 954, 27, doi: [10.3847/1538-4357/ace0ba](https://doi.org/10.3847/1538-4357/ace0ba)
- Barai, P., & de Gouveia Dal Pino, E. M. 2019, *MNRAS*, 487, 5549, doi: [10.1093/mnras/stz1616](https://doi.org/10.1093/mnras/stz1616)
- Barai, P., Murante, G., Borgani, S., et al. 2016, *MNRAS*, 461, 1548, doi: [10.1093/mnras/stw1389](https://doi.org/10.1093/mnras/stw1389)
- Barlow, T. A., Hamann, F., & Sargent, W. L. W. 1997, in *Astronomical Society of the Pacific Conference Series*, Vol. 128, *Mass Ejection from Active Galactic Nuclei*, ed. N. Arav, I. Shlosman, & R. J. Weymann, 13
- Baskin, A., & Laor, A. 2012, *MNRAS*, 426, 1144, doi: [10.1111/j.1365-2966.2012.21822.x](https://doi.org/10.1111/j.1365-2966.2012.21822.x)
- Baskin, A., Laor, A., & Stern, J. 2014, *MNRAS*, 445, 3025, doi: [10.1093/mnras/stu1732](https://doi.org/10.1093/mnras/stu1732)
- Begelman, M. C., McKee, C. F., & Shields, G. A. 1983, *ApJ*, 271, 70, doi: [10.1086/161178](https://doi.org/10.1086/161178)

- Berg, T. A. M., Ellison, S. L., Prochaska, J. X., Venn, K. A., & Dessauges-Zavadsky, M. 2015, *MNRAS*, 452, 4326, doi: [10.1093/mnras/stv1577](https://doi.org/10.1093/mnras/stv1577)
- Berti, E., & Volonteri, M. 2008, *ApJ*, 684, 822, doi: [10.1086/590379](https://doi.org/10.1086/590379)
- Bluck, A. F. L., Piotrowska, J. M., & Maiolino, R. 2023, *ApJ*, 944, 108, doi: [10.3847/1538-4357/acac7c](https://doi.org/10.3847/1538-4357/acac7c)
- Bollati, F., Lupi, A., Dotti, M., & Haardt, F. 2024, *A&A*, 690, A194, doi: [10.1051/0004-6361/202348538](https://doi.org/10.1051/0004-6361/202348538)
- Bowler, R. A. A., Hewett, P. C., Allen, J. T., & Ferland, G. J. 2014, *MNRAS*, 445, 359, doi: [10.1093/mnras/stu1730](https://doi.org/10.1093/mnras/stu1730)
- Braun, E., & Milgrom, M. 1989, *ApJ*, 342, 100
- Burbidge, E. M., & Burbidge, G. R. 1975, *ApJ*, 202, 287, doi: [10.1086/153975](https://doi.org/10.1086/153975)
- Bustamante, S., & Springel, V. 2019, *MNRAS*, 490, 4133, doi: [10.1093/mnras/stz2836](https://doi.org/10.1093/mnras/stz2836)
- Camenzind, M. 1986, *A&A*, 156, 137
- Chatzikos, M., Bianchi, S., Camilloni, F., et al. 2023, *RMxAA*, 59, 327, doi: [10.22201/ia.01851101p.2023.59.02.12](https://doi.org/10.22201/ia.01851101p.2023.59.02.12)
- Chelouche, D., & Netzer, H. 2003, *MNRAS*, 344, 233
- . 2005, *ApJ*, 625, 95, doi: [10.1086/429580](https://doi.org/10.1086/429580)
- Chen, C., Hamann, F., & Ma, B. 2021a, *ApJ*, 909, 208, doi: [10.3847/1538-4357/abe307](https://doi.org/10.3847/1538-4357/abe307)
- Chen, C., Hamann, F., Ma, B., & Murphy, M. 2021b, *ApJ*, 907, 84, doi: [10.3847/1538-4357/abcec5](https://doi.org/10.3847/1538-4357/abcec5)
- Chen, C., Hamann, F., Simon, L., & Barlow, T. 2018, *MNRAS*, 481, 3865, doi: [10.1093/mnras/sty2534](https://doi.org/10.1093/mnras/sty2534)
- Chen, C., Hamann, F., Simon, L., & Ma, B. 2019, *ApJ*, 887, 78, doi: [10.3847/1538-4357/ab53d8](https://doi.org/10.3847/1538-4357/ab53d8)
- Chen, C., Yi, W., He, Z., Hamann, F., & Ma, B. 2024, arXiv e-prints, arXiv:2410.20048, doi: [10.48550/arXiv.2410.20048](https://doi.org/10.48550/arXiv.2410.20048)
- Chen, Z., He, Z., Ho, L. C., et al. 2022, *Nature Astronomy*, 6, 339, doi: [10.1038/s41550-021-01561-3](https://doi.org/10.1038/s41550-021-01561-3)
- Costa, T., Sijacki, D., & Haehnelt, M. G. 2014, *MNRAS*, 444, 2355, doi: [10.1093/mnras/stu1632](https://doi.org/10.1093/mnras/stu1632)
- Dannen, R., Proga, D., Waters, T., & Dyda, S. 2024, *ApJ*, 961, 221, doi: [10.3847/1538-4357/ad0da5](https://doi.org/10.3847/1538-4357/ad0da5)
- de Kool, M., & Begelman, M. C. 1995, *ApJ*, 455, 448, doi: [10.1086/176594](https://doi.org/10.1086/176594)
- Dekker, H., D’Odorico, S., Kaufer, A., Delabre, B., & Kotzlowski, H. 2000, in *Society of Photo-Optical Instrumentation Engineers (SPIE) Conference Series*, Vol. 4008, *Optical and IR Telescope Instrumentation and Detectors*, ed. M. Iye & A. F. Moorwood, 534–545, doi: [10.1117/12.395512](https://doi.org/10.1117/12.395512)
- Di Matteo, T., Springel, V., & Hernquist, L. 2005, *Nature*, 433, 604
- Fechner, C., & Richter, P. 2009, *A&A*, 496, 31, doi: [10.1051/0004-6361/200810421](https://doi.org/10.1051/0004-6361/200810421)
- Foltz, C. B., Weymann, R. J., Morris, S. L., & Turnshek, D. A. 1987, *ApJ*, 317, 450
- Foltz, C. B., Weymann, R. J., Peterson, B. M., et al. 1986, *ApJ*, 307, 504
- Gallagher, S. C., Brandt, W. N., Wills, B. J., et al. 2004, *ApJ*, 603, 425, doi: [10.1086/381494](https://doi.org/10.1086/381494)
- Ganguly, R., & Brotherton, M. S. 2008, *ApJ*, 672, 102
- Ganguly, R., Eracleous, M., Charlton, J. C., & Churchill, C. W. 1999, *AJ*, 117, 2594
- Ganguly, R., Masiero, J., Charlton, J. C., & Sembach, K. R. 2003, *ApJ*, 598, 922, doi: [10.1086/379057](https://doi.org/10.1086/379057)
- Goldreich, P., & Sargent, W. 1976, *Comments on Astrophysics*, 6, 133
- Hall, P. B., Weiss, E., Brandt, W. N., & Mulholland, C. J. 2024, *MNRAS*, 528, 6496, doi: [10.1093/mnras/stae330](https://doi.org/10.1093/mnras/stae330)
- Hamann, F. 1997, *ApJS*, 109, 279
- Hamann, F., Barlow, T., Cohen, R. D., Junkkarinen, V., & Burbidge, E. M. 1997, in *Astronomical Society of the Pacific Conference Series*, Vol. 128, *Mass Ejection from Active Galactic Nuclei*, ed. N. Arav, I. Shlosman, & R. J. Weymann, 19–+
- Hamann, F., Kanekar, N., Prochaska, J. X., et al. 2011, *MNRAS*, 410, 1957. <https://arxiv.org/abs/1008.3728>
- He, Z., Liu, G., Wang, T., et al. 2022, *Science Advances*, 8, eabk3291, doi: [10.1126/sciadv.abk3291](https://doi.org/10.1126/sciadv.abk3291)
- He, Z., Chen, Z., Liu, G., et al. 2024, *Science China Physics, Mechanics, and Astronomy*, 67, 129512, doi: [10.1007/s11433-024-2475-7](https://doi.org/10.1007/s11433-024-2475-7)
- Helfand, D. J., White, R. L., & Becker, R. H. 2015, *ApJ*, 801, 26, doi: [10.1088/0004-637X/801/1/26](https://doi.org/10.1088/0004-637X/801/1/26)
- Hopkins, P. F., & Elvis, M. 2010, *MNRAS*, 401, 7. <https://arxiv.org/abs/0904.0649>
- Horne, K. 1986, *PASP*, 98, 609, doi: [10.1086/131801](https://doi.org/10.1086/131801)
- Juráňová, A., Costantini, E., Kriss, G. A., et al. 2024, *A&A*, 686, A99, doi: [10.1051/0004-6361/202449544](https://doi.org/10.1051/0004-6361/202449544)
- Kauffmann, G., & Haehnelt, M. 2000, *MNRAS*, 311, 576
- Korista, K. T., Voit, G. M., Morris, S. L., & Weymann, R. J. 1993, *ApJS*, 88, 357, doi: [10.1086/191825](https://doi.org/10.1086/191825)
- Krolik, J. H., & Begelman, M. C. 1986, *ApJL*, 308, L55, doi: [10.1086/184743](https://doi.org/10.1086/184743)
- Lewis, T. R., & Chelouche, D. 2023, *ApJ*, 945, 110, doi: [10.3847/1538-4357/acb541](https://doi.org/10.3847/1538-4357/acb541)
- Lin, Y.-R., & Lu, W.-J. 2020a, *MNRAS*, 497, 1457, doi: [10.1093/mnras/staa2037](https://doi.org/10.1093/mnras/staa2037)
- . 2020b, *ApJ*, 899, 155, doi: [10.3847/1538-4357/aba9db](https://doi.org/10.3847/1538-4357/aba9db)
- Lu, W.-J., & Lin, Y.-R. 2020, *ApJL*, 895, L44, doi: [10.3847/2041-8213/ab9303](https://doi.org/10.3847/2041-8213/ab9303)

- Ma, B., & Ge, J. 2019, MNRAS, 484, 760, doi: [10.1093/mnras/stz028](https://doi.org/10.1093/mnras/stz028)
- Milne, E. A. 1926, MNRAS, 86, 459, doi: [10.1093/mnras/86.7.459](https://doi.org/10.1093/mnras/86.7.459)
- Murphy, M. T., Kacprzak, G. G., Savorgnan, G. A. D., & Carswell, R. F. 2019, MNRAS, 482, 3458, doi: [10.1093/mnras/sty2834](https://doi.org/10.1093/mnras/sty2834)
- Murphy, M. T., Tzanavaris, P., Webb, J. K., & Lovis, C. 2007, MNRAS, 378, 221, doi: [10.1111/j.1365-2966.2007.11768.x](https://doi.org/10.1111/j.1365-2966.2007.11768.x)
- Murray, N., Chiang, J., Grossman, S. A., & Voit, G. M. 1995, ApJ, 451, 498
- Mushotzky, R. F., Solomon, P. M., & Strittmatter, P. A. 1972, ApJ, 174, 7, doi: [10.1086/151463](https://doi.org/10.1086/151463)
- Naddaf, M. H., Martinez-Aldama, M. L., Marziani, P., et al. 2023, A&A, 675, A43, doi: [10.1051/0004-6361/202245698](https://doi.org/10.1051/0004-6361/202245698)
- Netzer, H. 2006, ApJL, 652, L117, doi: [10.1086/510067](https://doi.org/10.1086/510067)
- Netzer, H., & Laor, A. 1993, ApJL, 404, L51, doi: [10.1086/186741](https://doi.org/10.1086/186741)
- Netzer, H., Goad, M. R., Barth, A. J., et al. 2024, ApJ, 976, 59, doi: [10.3847/1538-4357/ad8160](https://doi.org/10.3847/1538-4357/ad8160)
- O'Meara, J. M., Lehner, N., Howk, J. C., et al. 2015, AJ, 150, 111, doi: [10.1088/0004-6256/150/4/111](https://doi.org/10.1088/0004-6256/150/4/111)
- Pâris, I., Petitjean, P., Aubourg, É., et al. 2018, A&A, 613, A51, doi: [10.1051/0004-6361/201732445](https://doi.org/10.1051/0004-6361/201732445)
- Pelletier, G., & Pudritz, R. E. 1992, ApJ, 394, 117, doi: [10.1086/171565](https://doi.org/10.1086/171565)
- Petitjean, P., Ledoux, C., & Srianand, R. 2008, A&A, 480, 349, doi: [10.1051/0004-6361:20078607](https://doi.org/10.1051/0004-6361:20078607)
- Petitjean, P., Rauch, M., & Carswell, R. F. 1994, A&A, 291, 29
- Piskunov, N. E., & Valenti, J. A. 2002, A&A, 385, 1095, doi: [10.1051/0004-6361:20020175](https://doi.org/10.1051/0004-6361:20020175)
- Prochaska, J. X., & Hennawi, J. F. 2009, ApJ, 690, 1558, <https://arxiv.org/abs/0806.0862>
- Prochaska, J. X., Hennawi, J. F., & Herbert-Fort, S. 2008, ApJ, 675, 1002, doi: [10.1086/526508](https://doi.org/10.1086/526508)
- Prochaska, J. X., O'Meara, J. M., Fumagalli, M., Bernstein, R. A., & Burles, S. M. 2015, ApJS, 221, 2, doi: [10.1088/0067-0049/221/1/2](https://doi.org/10.1088/0067-0049/221/1/2)
- Proga, D. 2007, ApJ, 661, 693, doi: [10.1086/515389](https://doi.org/10.1086/515389)
- Proga, D., & Kallman, T. R. 2004, ApJ, 616, 688
- Proga, D., Stone, J. M., & Kallman, T. R. 2000, ApJ, 543, 686
- Quintin, E., Webb, N. A., Georgantopoulos, I., et al. 2024, A&A, 687, A250, doi: [10.1051/0004-6361/202348317](https://doi.org/10.1051/0004-6361/202348317)
- Sargent, W. L. W., Boksenberg, A., & Steidel, C. C. 1988, ApJS, 68, 539, doi: [10.1086/191300](https://doi.org/10.1086/191300)
- Scannapieco, E., & Oh, S. P. 2004, ApJ, 608, 62
- Scargle, J. D. 1973, ApJ, 179, 705, doi: [10.1086/151910](https://doi.org/10.1086/151910)
- Shaban, F., Siemiginowska, A., Suleiman, R. M., El-Nawawy, M. S., & Ali, A. 2022a, Journal of High Energy Astrophysics, 36, 152, doi: [10.1016/j.jheap.2022.10.002](https://doi.org/10.1016/j.jheap.2022.10.002)
- . 2022b, Journal of High Energy Astrophysics, 36, 152, doi: [10.1016/j.jheap.2022.10.002](https://doi.org/10.1016/j.jheap.2022.10.002)
- Shen, Y., Richards, G. T., Strauss, M. A., et al. 2011, ApJS, 194, 45, doi: [10.1088/0067-0049/194/2/45](https://doi.org/10.1088/0067-0049/194/2/45)
- Silk, J., & Rees, M. J. 1998, A&A, 331, L1
- Srianand, R., Petitjean, P., Ledoux, C., & Hazard, C. 2002, MNRAS, 336, 753, doi: [10.1046/j.1365-8711.2002.05792.x](https://doi.org/10.1046/j.1365-8711.2002.05792.x)
- Turnshek, D. A., Weymann, R. J., Carswell, R. F., & Smith, M. G. 1984, ApJ, 277, 51, doi: [10.1086/161670](https://doi.org/10.1086/161670)
- Vilkoviskij, E. Y., & Irwin, M. J. 2001, MNRAS, 321, 4, doi: [10.1046/j.1365-8711.2001.03985.x](https://doi.org/10.1046/j.1365-8711.2001.03985.x)
- Wang, S., Liu, J., Qiu, Y., et al. 2016, ApJS, 224, 40, doi: [10.3847/0067-0049/224/2/40](https://doi.org/10.3847/0067-0049/224/2/40)
- Weedman, D., Sargsyan, L., Lebouteiller, V., Houck, J., & Barry, D. 2012, ApJ, 761, 184, doi: [10.1088/0004-637X/761/2/184](https://doi.org/10.1088/0004-637X/761/2/184)
- Weymann, R. J., Morris, S. L., Foltz, C. B., & Hewett, P. C. 1991, ApJ, 373, 23
- Weymann, R. J., Williams, R. E., Peterson, B. M., & Turnshek, D. A. 1979, ApJ, 234, 33
- Yi, W., Hall, P. B., Yuan, Z., et al. 2024, ApJS, 271, 61, doi: [10.3847/1538-4365/ad2a42](https://doi.org/10.3847/1538-4365/ad2a42)
- Zechmeister, M., Anglada-Escudé, G., & Reiners, A. 2014, A&A, 561, A59, doi: [10.1051/0004-6361/201322746](https://doi.org/10.1051/0004-6361/201322746)